Cooperative and fully reversible photocatalytic colour switching activation in graphene-copper-TiO_2 nanoparticles

DM Tobaldi,[a,*] L Lajaunie,[b,c] D Dvoranová,[d] B Figueiredo,[e] MP Seabra,[a] JJ Calvino,[b,c] V Brezová,[d] JA Labrincha[a]

[a] *Department of Materials and Ceramic Engineering and CICECO–Aveiro Institute of Materials, University of Aveiro, Campus Universitário de Santiago, 3810–193 Aveiro, Portugal*

[b] *Departamento de Ciencia de los Materiales e Ingeniería Metalúrgica y Química Inorgánica, Facultad de Ciencias, Universidad de Cádiz, Campus Río San Pedro S/N, Puerto Real 11510, Cádiz, Spain*

[c] *Instituto Universitario de Investigación de Microscopía Electrónica y Materiales (IMEYMAT), Facultad de Ciencias, Universidad de Cádiz, Campus Río San Pedro S/N, Puerto Real 11510, Cádiz, Spain*

[d] *Institute of Physical Chemistry and Chemical Physics, Faculty of Chemical and Food Technology, Slovak University of Technology in Bratislava, Radlinského 9, Bratislava, SK-812 37, Slovakia*

[e] *Graphenest, Lugar da Estação, Edifício Vouga Park 3740–070, Paradela do Vouga, Portugal*

Abstract

Nanostructured systems showing reversible colour switching are envisaged to play a significant role in photo-switches, photo-optical sensors, smart windows, displays, optical storage memories. Most of the materials exhibiting reversible colour switching are organic compounds. However, their UV-light activation, low thermal and chemical stability, as well as harmful synthesis methods, are of limit for their extensive use. In this research, we have created an inorganic switchable photochromic material exploiting TiO_2 ability of creating an exciton upon excitation, copper as the chromophore, and graphene's extraordinarily high electron mobility. Our material showed itself to be able to work under visible-light, its photochromic property being three times faster than conventional titania based photochromic materials, reaching a stable change in colouration after only 30 mins of visible-light irradiation (*versus* > 120 min in conventional Cu-TiO_2). With the addition of just 1 wt% graphene, the material exhibited a staggeringly stable photochromic switching over repeated cycles. These results relate to the best previously reported values for any form of TiO_2-based photochromic material. This is therefore an excellent candidate for smart self-cleaning windows, and other chromic devices and applications.

KEYWORDS: photocatalytic colour switching; visible-light; graphene; copper; smart-materials

*Corresponding author. Tel.: +351 234 370 041

E-mail addresses: david.tobaldi@ua.pt; david@davidtobaldi.org (DM Tobaldi)

1. Introduction

When a material exhibits a reversible change in colour upon an external stimulus, it is named *chromic material*. This is an important class of materials because of its cutting edge applications, such as: sensors, memory devices, information displays, signage technologies, and security features.[1] Temperature, chemicals, electricity, mechanical, impact, light might be the external stimuli. Therefore, we can talk about: thermochromic, electrochromic, piezochromic and photochromic materials.[2] Light is of certain importance as the external stimulus to trigger (photo)chromism. Indeed, unlike other stimuli, light has a non-invasive character and we can easily control parameters like the energy, intensity, exposure area, time of irradiation.[3] Thus, photochromic materials are of an extreme significance in making the smart materials of the future. As the word itself says, photochromism derives from the transliteration of the ancient Greek words "*φῶς*" (light) and "*χρώμα*" (colour). Therefore, photochromism can be defined as the reversible change in colour and/or optical absorption spectra under electromagnetic radiation.[4] Reversibility of the colouration can be triggered by exposing the material to light of a different wavelength compared to that the caused the initial change in colour,[5] by chemical oxidation,[4] or by giving thermal energy in the dark.[6] Usually organic compounds exhibit reversible colour switching upon light exposure. Organic compounds displaying photochromism are: diarylethenes, spiropyrans, azobenzenes, spirooxazines.[7] That photochromic response is given by a wide range of reactions, such as: pericyclic reactions, cis–trans isomerisations, or intramolecular hydrogen transfer.[8] However, organic photochromic materials involve complex synthesis methods, are not thermally stable and have been shown to possess weak colour switching when in solid media.[9] That is the reason why inorganic compounds as photochromic materials are gaining momentum – WO_3, MoO_3, silver halides, oxides of Group 4 and 5 (*i.e.*, TiO_2, V_2O_5, Nb_2O_5) have indeed shown to exhibit reversible photochromism.[4] However, elements like nickel and tungsten are linked to potential environmental and health hazard.[10] Therefore, titanium dioxide nanoparticles are of significance amid the metal oxides listed before. Aside from being an abundant, low-cost, non-toxic and stable oxide, TiO_2 nanoparticles are also able to generate an exciton upon excitation – *i.e.*, the photocatalytic phenomenon.[11] Still, the wide band-gap of TiO_2 limits its range of application to the UVA part of the electromagnetic spectrum. Indeed, Wang and co-authors have recently shown a reversible photocatalytic colour switching in organic-inorganic hybrids made of TiO_2 and organic dyes.[12,13] Nevertheless, the reduction reaction, responsible for the change in colour, was restricted to UV-light irradiation, thus reducing the application range. To (partly) overcome this issue, it has been recently proved that a type-II (staggered) band alignment of ~0.4 eV exists between anatase and rutile TiO_2 polymorphs when they are in form of a hetero-junction – with anatase possessing the higher electron affinity.[14] Recently, Maheu and colleagues confirmed (*via* combined UPS and UV spectroscopy) this outcome to happen also in anatase-rutile nanopowders.[15]

However, TiO_2 is transparent to most of the visible radiation region, its electronic configuration retaining zero 3*d* electrons.[16] One of the strategies to make a (TiO_2-based) material showing reversible photocatalytic colour switching is to decorate titania's surface with element having more than one oxidation state. At this regard, copper is a much interesting candidate. Cu is a 3*d* transition metal; copper-based materials are able to promote and undergo a variety of reactions owing to copper wide range of oxidation states – Cu^0, Cu^{1+}, Cu^{2+}, and Cu^{3+}.[17]

Since the first publication by Geim and Novoselov,[18] graphene swiftly raised as "*The star*" on the horizon of materials science.[19] This interest certainly arose because of graphene's outshining electronic properties,[20] having high mobility of charge carriers – higher than 200,000 $cm^2.V^{-1}s^{-1}$ [21,22] – and high in-plane thermal conductivity (1,000–5,300 $W.mK^{-1}$).[23] Interestingly, semiconductor and metal nanoparticles can be successfully "anchored" on 2D carbon support to improve the catalytic activity.[24]

In this research work, we have used that strategy to improve the reversibility of photocatalytic colour switching in copper-graphene modified TiO_2 nanoparticles – the full-blown limit of that material.[25] The exciton has been generated upon TiO_2 excitation; graphene has been exploited has a highway for the exciton mobility, whilst copper has been used as the chromophore.[26] Obtained results showed that TiO_2 specimen modified with 1 mol% Cu and graphene (0.5 and 1.0 wt%) exhibited fast photocatalytic colour switching under exposure of a white light emitting diode lamp, attaining a stable colouration after 30 min (*versus* > 120 min of copper-TiO_2). Most importantly, the reversibility of photochromic switching showed itself to be staggeringly stable over repeated cycles, when stored at 100 °C in dark.

2. Experimental section

2.1 Sample preparation

An aqueous sol-gel method was followed for the synthesis of TiO_2-based photochromic materials.[27] To do the Cu-graphene-modified TiO_2, stoichiometric amounts of copper(II) nitrate trihydrate (Sigma-Aldrich, ≥ 98.5%) were added to the TiO_2-based sol when this had a 1 M concentration. The concentration of copper was constrained at 1 mol%, following on from our earlier studies.[26] 0.5 and 1 wt% of graphene nanoplatelets dispersed in ethanol (kindly supplied by Graphenest) were also added at this step to the 1 M sol. The sols were dried in an oven at 80 °C, and then the dried gels were thermally treated following thermal cycles reaching two maximum temperatures. (i) 250 °C with a heating rate of 15 °C min^{-1}, pre-heating the furnace at 200 °C, with a 8 h dwell time; (ii) 450 °C, with a heating rate of 5 °C min^{-1}, with 2 h dwell time. Specimens were referred to as: **Cu-Gx/Y** were *x* stands for the graphene wt% (0.5 or 1.0 wt%), and *Y* is a number indicating the maximum temperature reached (*i.e.* 250 or 450). For instance, the TiO_2 sol

in which 1 mol% Cu and 0.5 wt% graphene were added, and thermally treated at 450 °C / 2h will be referred to as: **Cu-G0.5/450**.

2.2 Sample characterisation

The mineralogical composition of the prepared specimens was revealed by means of X-ray powder diffraction (XRPD). The relative fractions of crystalline phases were determined *via* Rietveld refinements of the XRPD data. The XRPD patterns were collected at room temperature on a θ/θ diffractometer (PANalytical X'Pert Pro, NL), equipped with a fast RTMS detector (PIXcel 1D, PANalytical), with Cu K_α radiation (45 kV and 40 mA, 20–80 °2θ range, with a virtual step scan of 0.02 °2θ, and virtual time per step of 200 s). The Rietveld data analysis for obtaining semi-quantitative phase analysis (QPA) information was assessed using the GSAS software package and its graphical interface EXPGUI.[28,29] The instrumental broadening was obtained from the refinement of LaB_6 standard (NIST SRM 660b) and included in all of the Rietveld refinements. The refinement strategy that we followed has been reported in previous works.[27] XRPD was used also to obtain microstructural information. At this purpose, the same instrument and setup as per the QPA was employed, but XRPD patterns were recorded in the 20–145 °2θ range, with a virtual step-scan of 0.1 °2θ, and virtual time per step of 500 s, so to deal with data with a higher signal-to-noise ratio. The whole powder pattern modelling (WPPM),[30] as implemented in the PM2K software package,[31] was used for the microstructural analysis of the diffraction data. WPPM is a novel yet well-established method for extracting microstructural features from a diffraction pattern. It employs XRPD data by describing each observed peak profile as a convolution of instrumental and sample-related physical effects. The corresponding model parameters are then directly refined on the observed data.[32] In this work we adopted the same modelling approach as that we described in previous researches, assuming crystalline domains be spherical, and their diameter distributed according to a log-normal curve.[27]

Raman spectra were acquired on a RFS 100/S (Bruker, DE) equipped with a 1,064 nm Nd:YAG laser as the excitation source, in the 50–1,800 cm^{-1} wavenumber range, with 2 cm^{-1} in resolution.

2.2.1 Optical properties: reversible photocatalytic colour switching activation

The changes in the optical properties triggered by light (*i.e.* the photocatalytic colour switching) were investigated by way of diffuse reflectance spectroscopy (DRS). Optical spectra were recorded on a Shimadzu UV-3100 spectrometer (JP), equipped with an integrating sphere, and a white reference material made of Spectralon; UV–vis spectral range was explored (250–850 nm), using 0.2 nm in resolution. To analyse the photochromic properties, 0.1 g of specimen was exposed to a white light emitting diode (LED) (Philips warm

white, 2700 K LED bulb, 9.5 W). A protocol described in detail was severely followed to ensure comparable data.[25,26,33] The intensity of the radiation reaching the samples was measured with a radiometer (Delta OHM, HD2302.0, IT), and it was estimated to be 5.0 mW.cm^{-2} in the visible spectral region (>400 nm, being nil in the UVA) – irradiation times were consecutive and absolute. DR data were converted into pseudoabsorption spectra $F(R)$ by means of the Kubelka–Munk transformation:[34] $F(R) = \alpha = (1 - R)^2/2R$, where R is the DR. As photochromism is reversible by definition, its reversibility was studied by exposing fresh unexposed samples to visible light (as above) for periods ranging from 30 to 15 s, at room temperature and then recording immediately their DR spectra. They were then placed in a dark oven at 100 °C for 15 or 30 min to aid reversing the process, and the optical spectra were measured again. The degree of photoswitching has been defined as the difference between the maximum value in reflectance at time zero (R_0), and the reflectance after each irradiation/annealing cycle (R_t): ΔR_t (%) = $[(R_0 - R_t)/R_0 \times 100]$.[35]

3. Results and discussion

3.1 XRPD and HR-TEM analyses

XRPD semi QPA data are listed in Table 1. A graphical output of a Rietveld refinement is shown in Figure S1 (Supporting Information File). Unmodified titania dried gel thermally treated at 205 °C / 8h led to the formation of anatase (92.8 wt%), rutile (5.1 wt%) and brookite (2.1 wt%) TiO_2 polymorphs. Addition of 1 mol % copper and graphene (0.5 and 1.0 wt%) to the system delayed the anatase-to-rutile phase transition (ART). However, **Cu-G0.5/250** and **Cu-G1.0/250** virtually had the same mineralogical composition, thus one can infer that graphene had no (or little) influence on the ART,[36] a nucleation-and-growth phenomenon.[37] The same conclusion can be drawn for the specimens subjected to the 450 °C / 2h thermal cycle: ART was delayed as well, and graphene had virtually no influence on it. Copper did not enter TiO_2 structure, for crystallochemical reasons;[26] still it favoured a grain-boundary pinning, thus delaying the ART.[33]

Table 1 – Rietveld agreement factors and phase fraction (wt%) of TiO_2 polymorphs in the prepared specimens.[a]

Sample	No. of	Agreement factors			Phase composition (wt%)		
	variables	$R(_F^2)$ (%)	R_{wp} (%)	χ^2	anatase	rutile	brookite
TiO_2/250	13	2.03	3.29	1.41	92.8(1)	5.1(4)	2.1(2)
Cu-G0.5/250	20	2.89	3.32	1.56	94.4(1)	2.8(3)	2.8(2)
Cu-G1.0/250	20	2.55	3.19	1.56	95.5(1)	2.1(2)	2.3(2)
TiO_2/450	20	3.60	3.34	1.97	70.8(1)	19.5(1)	9.7(2)
Cu-G0.5/450	21	6.32	3.32	1.73	89.6(1)	8.6(2)	1.7(2)
Cu-G1.0/450	22	5.54	2.90	1.66	89.0(1)	9.8(2)	1.2(2)

[a] There were 2285 observations for every refinement; the number of anatase, rutile and brookite reflections was 32, 31 and 154, respectively

Table 2 – WPPM agreement factors, average diameter of the crystalline domains and polydispersity index (PDI).

Sample	Agreement factors			Mean crystalline domain diameter (nm)		PDI	
	R_{wp} (%)	R_{exp} (%)	χ^2	anatase	rutile	anatase	rutile
TiO_2/250	3.65	3.38	1.08	4.4±0.1	8.7±1.4	0.25±0.01	0.30±0.02
Cu-G0.5/250	2.44	2.17	1.13	3.2±0.1	8.6±0.1	0.39±0.01	0.31±0.06
Cu-G1.0/250	2.43	2.16	1.12	3.5±0.2	8.6±0.2	0.35±0.01	0.31±0.05
TiO_2/450*	2.72	2.30	1.18	8.7±0.2	14.4±0.6	0.17±0.08	0.18±0.04
Cu-G0.5/450	2.80	2.29	1.22	7.1±0.3	9.3±0.5	0.21±0.01	0.40±0.05
Cu-G1.0/450	2.52	2.22	1.13	7.4±0.5	9.8±0.7	0.21±0.01	0.38±0.01

* Values from reference [33].

Microstructural features of the specimens, as extracted with the WPPM modelling, are listed in Table 2, and graphically reported in Figure S2a-d. A graphical output of a WPPM modelling is shown in Figure S3. Anatase crystalline domains in unmodified TiO_2 thermally treated at 250 °C / 8h (**TiO_2/250**) have an average diameter of 4.4 nm, those of rutile 8.7 nm. Consistent with QPA analysis results, addition of copper and graphene seemed to have dictated a decrease in the nucleation-and-growth of anatase, leading to a smaller size of the diameter domains. As a matter of fact, the average crystalline domain diameters of anatase in **Cu-G0.5/250** and **Cu-G1.0/250** are 3.2 and 3.5 nm, respectively. This is reflected by their moderately polydispersity indices (0.1<PDI<0.4).[38] On the other hand, neither copper nor graphene additions had virtually any influence in the nucleation-and-growth of rutile crystalline domains, the average diameter of these being 8.7, 8.6 and 8.6 nm in **TiO2/250**, **Cu-G0.5/250** and **Cu-G1.0/250**, respectively. An increase in the thermal treatment (*i.e.* 450 °C with 2 h dwell time), led to an increase in the average diameter of anatase and rutile domains, following to nucleation-and-growth process, these being 8.7 and 14.4 nm, respectively, in **TiO_2/450**. Likewise the specimens thermally treated at 250 °C, addition of copper and graphene had an influence in retarding that nucleation-and-growth process. Indeed, anatase crystalline domains in **Cu-G0.5/450** and **Cu-G1.0/450** had average diameters equal to 7.1 and 7.4 nm, respectively; those of rutile were 9.3 and 9.8 nm.

Raman spectra showing a general view of the specimens are reported in Figure S4a,b; in them, anatase Raman active modes located at 144 (E_g), 399 (B_{1g}), 519 (A_{1g}, B_{1g}) and 639 cm^{-1} (E_g) are visible.[39] In the specimens thermally treated at 450 °C / 2 h, Figure S4b (**Cu-G0.5/450** and **Cu-G1.0/450**) it is also detectable the E_g Raman mode of rutile, at around 447 cm^{-1}.[39] Furthermore, as listed in Table S1, the Raman E_g mode of anatase is shifted toward higher energies in all of the specimens modified with copper and graphene. Thus this confirms their reduced dimensions (and increased disorder),[40] compared to that of unmodified anatase. Raman spectra in the 950–1,800 cm^{-1} energy region are shown in Figure X1a,b. In the specimens thermally treated at 250 °C / 8h is present also another Raman line at approximately 1,050 cm^{-1}, Figure X1a, being assigned to C–O stretching, a legacy of unreacted organic moieties.[41] Moreover, the major bands assigned to graphene (*i.e.*, the *G* band together with *D* and a weak *D´* band) are present in the samples, see Figure X1a,b. The presence of *D* and *D´* Raman bands is an indication of irregular edge disorders and oxidised dangling bonds.[42] Interestingly, the *D* line, related to disordered carbon, is located at around 1,300 cm^{-1}, this being a common characteristic of single-wall carbon nanotube,[43] therefore consistent with HR-TEM observations.

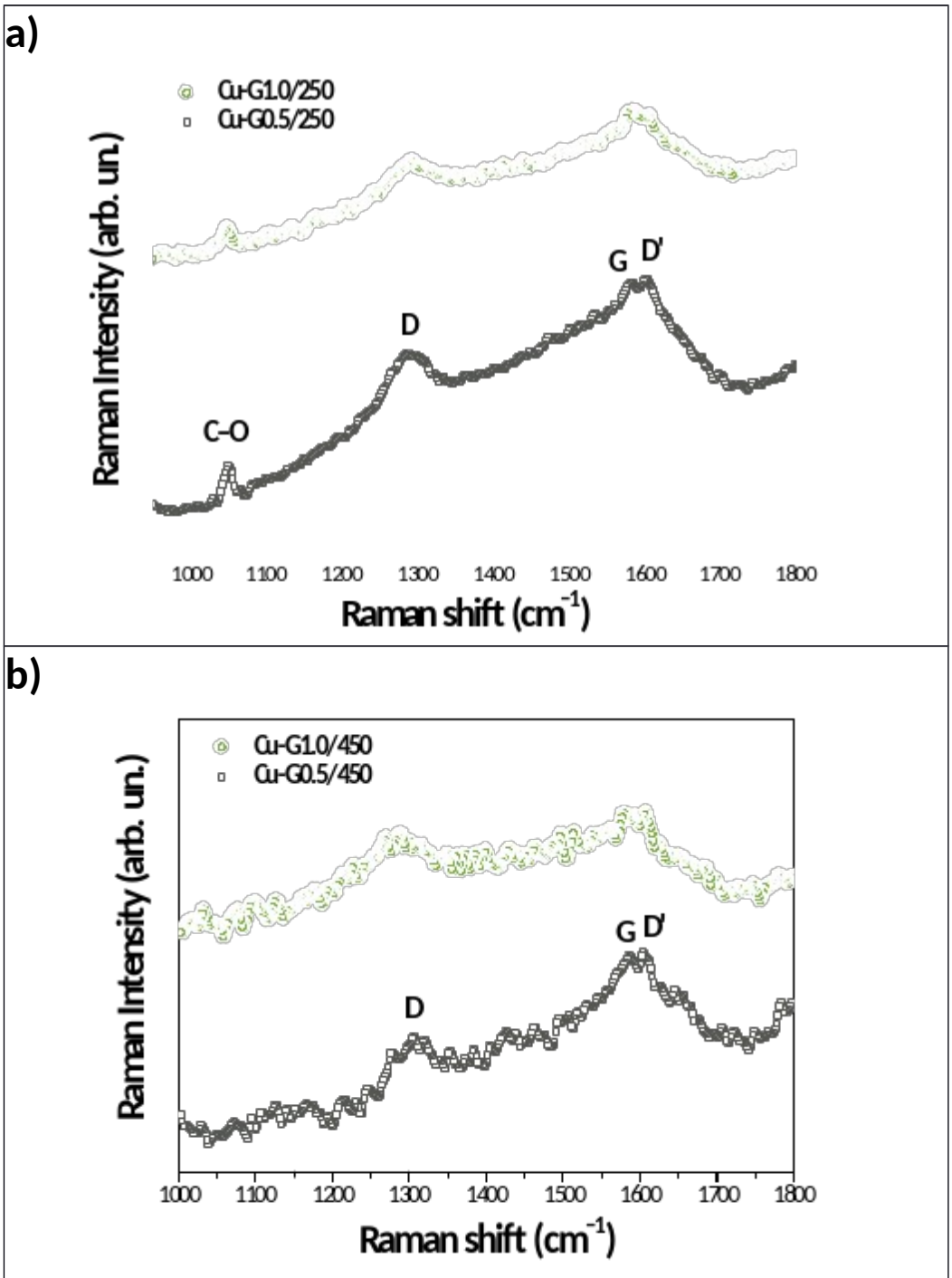

Figure X1 – Raman spectra of: a) specimens thermally treated at 250 °C / 8h; b) specimens thermally treated at 450 °C / 2h

3.2 Optical Properties: Photocatalytic aided colour switching

Optical spectra of fresh unexposed specimens are reported in Figure S5. Spectra of the specimens thermally treated at 250 °C / 8h and 450 °C / 2h all show similar characteristics. The absorption band at around <3.2 eV is assigned to the band-to-band transition in TiO_2.[44] The absorption feature located at around 2.75 eV, belongs to interfacial charge transfer (IFCT), that is: the electron transferring (under visible-light irradiation)

from the valence band of TiO_2 to the Cu_xO and/or graphene clusters that are grafted at the interface with titania.[45] Indeed, it is reasonable to propose the IFCT to happen also amongst graphene and TiO_2,[46] being that absorption feature more intense in the specimens with 1.0 wt% graphene, at both the thermal treatment temperatures. The strong absorption band detected at lower energies (<2.25 eV) and centred at ~1.5 eV, belongs to *d*–*d* electronic transition in Cu^{2+}.[47]

Irradiation of Cu-graphene modified TiO_2 specimens with the white-light emitting LED induced changes to their optical spectra, as shown in Figure S6 and in Figure X2. Looking at the specimens thermally treated at 250 °C / 8h, Figure S6a,b, it is evident the growth in intensity of the absorption feature due to Cu^{2+}/graphene-TiO_2 IFCT with the white-light emitting LED irradiation time. However, little changes in the Cu^{2+} *d*–*d* transitions happened. This likely means that, under visible-light irradiation time, specimens thermally treated at 250 °C / 8 h do not generate an exciton.[27] As a consequence, Cu^{2+} has not (or not entirely) been reduced to Cu^{+} by photocatalysis. Still, we can hypothesise that visible-light irradiation was able to initiate IFCT amongst electrons in the valence band of TiO_2 that are excited to copper/graphene clusters at the interface,[45] being (mostly) responsible for the increase in the absorption feature displayed in Figure S6a,b and inset in Figure S7a,b, and of the little Cu^{2+} reduction (main Figure S7a,b).

On the other hand, when specimens thermally treated at 450 °C / 2 h are subjected to (consecutive) visible-light irradiation time an exciton is generated,[27] and more complex changes to their optical spectra occurred. As displayed in Figure X2a,b, an increase in the visible-light irradiation time led to: (i) a progressive decrease in the absorption band due to Cu^{2+} *d*–*d* transitions, until it completely disappeared – at around 30 min irradiation time; (ii) a simultaneous increase in the absorption feature owing to Cu^{2+}/graphene-TiO_2 IFCT (up to 30-45 min irradiation time); (iii) the appearance, after approximately 30 min irradiation time, of a new absorption band, centred at around 2.25 eV (~550 nm), and belonging to the band-gap transition in Cu_2O.[48] [In 1 mol% copper TiO_2, adopting the very same exposure condition, we did not observe the appearance of that band belonging to the interband transition in Cu_2O: this suggests that under white-light irradiation the electron transport was not enough to generate that band, see reference [26] and Figure S8 for a direct visual comparison with Figure X2.] This behaviour is explained taking into consideration that an exciton is formed upon TiO_2 visible-light irradiation (*i.e.*, photocatalysis).[11] The photo-generated electron in the conduction band of TiO_2 is then able to migrate to CuO that is clustered around titania. This, concurrently with the IFCT mechanism, led to a complete reduction of Cu^{2+} to Cu^{+} – this is shown by the complete disappearance of the Cu^{2+} *d*–*d* band in favour of the appearance and growth in intensity of the Cu_2O interband absorption feature, as displayed in Figure X2b. In other words, we assisted at a cooperative photocatalytic / IFCT assisted change in colour.

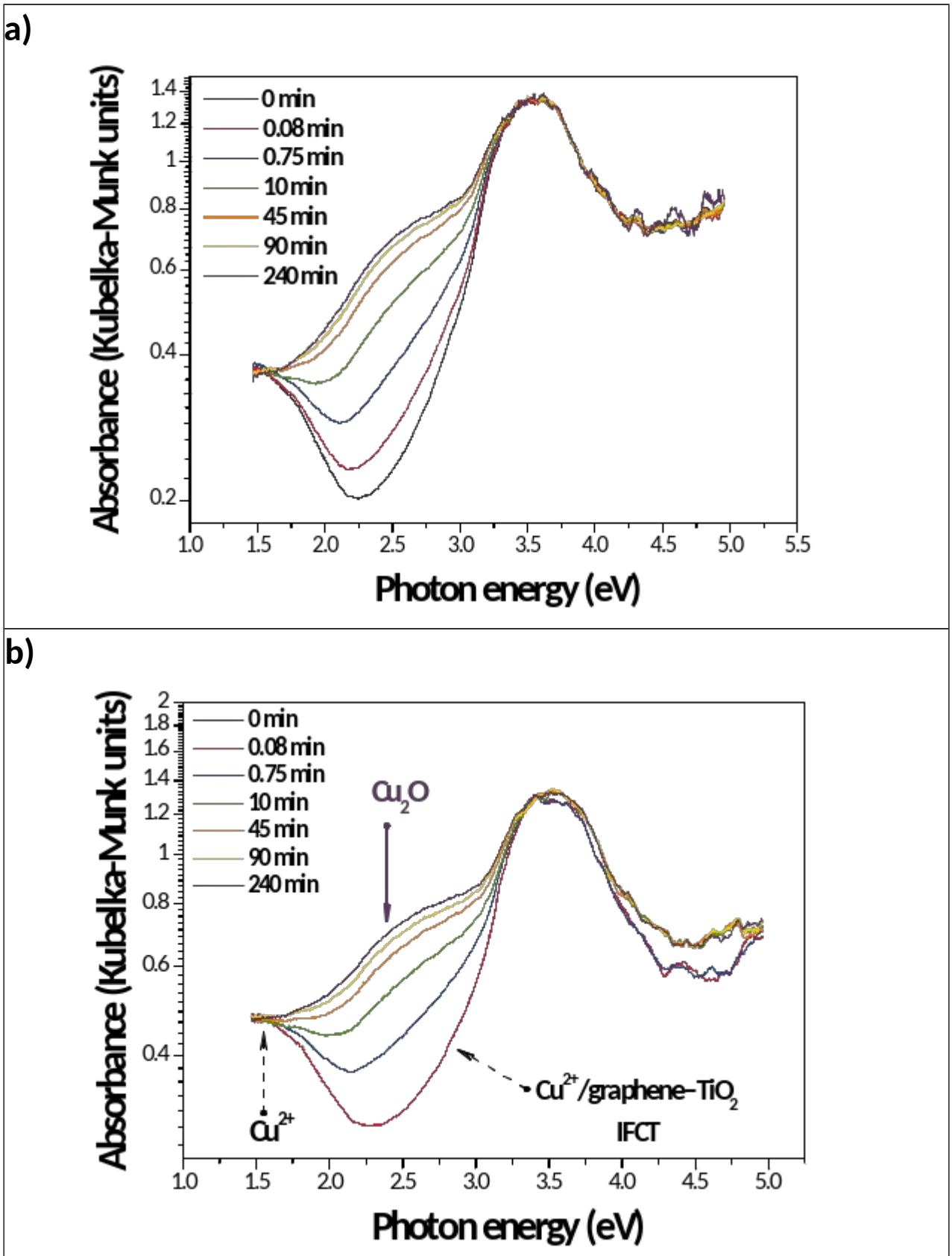

Figure X2 – Optical spectra (absorbance *versus* energy) of: a) **Cu-G0.5/450**, and b) **Cu-G1.0/450**, irradiated with the visible-light emitting LED for 0, 0.08, 0.75, 10.00, 45.00, 90.00, and 240.00 min. The *y*-axis is in log-scale to highlight the increase and disappearance of the absorption feature due to Cu^{2+}/graphene-TiO_2 IFCT, the disappearance of the band due to Cu^{2+} *d*–*d* transitions, and the appearance of the Cu_2O interband absorption in lieu of these two absorption bands.

The optical evolution of the specimens with visible-light irradiation time was followed to have quantitative information about the decrease of the integrated area of the absorption band belonging to Cu^{2+} *d–d* electronic transition, as well as the increase/formation of those due to IFCT/Cu_2O. Quantitative results are reported in Figure S7a,b, and Figure X3a,b.

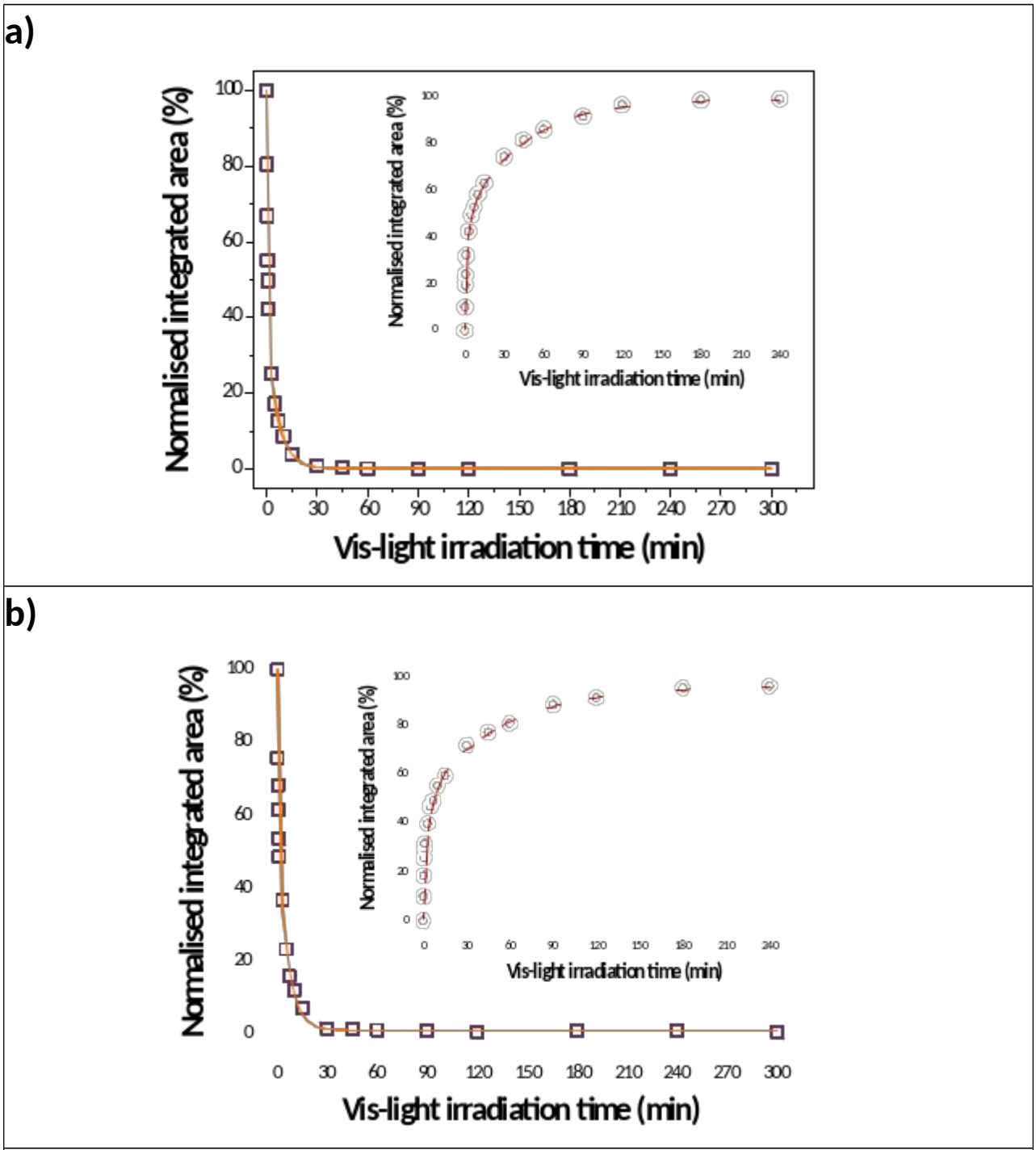

Figure X3 – a) Evolution of the decrease in the area due to Cu^{2+} *d–d* transition band area in **Cu-G0.5/450**, following visible-light irradiation (R^2 of the 3rd order exponential function was 0.999); the inset reports the evolution of the increase in the integrated area due to IFCT band and the simultaneous generation/growth of the interband absorption due to Cu_2O, same specimen, R^2 = 0.999. b) Evolution of the decrease in the area due to Cu^{2+} *d–d* transition band area in **Cu-G1.0/450**, following visible-light irradiation (R^2 of the 3rd order exponential function was 0.998); the inset reports the evolution of the increase in the integrated area due to IFCT band and the simultaneous generation/growth of the interband absorption due to Cu_2O, same specimen, R^2 = 0.999.

Specimens thermally treated at 250 °C / 8h, Figure S7a,b, experienced a weaker change in colour (mostly due to IFCT) compared to those thermally treated at 450 °C / 2h. For that reason, in this work will be discussed the photocatalytic colour switching for specimens treated at 450 °C. Results reported in Figure X3a,b suggest that the decrease in the Cu^{2+} absorption band as well as the IFCT/CuO growth/formation follow a third-order exponential function. On the contrary, copper-modified titania, gave the best fit with a double-exponential function,[26] yet Manno and co-authors reported a first-order kinetic process for a Ag-TiO_2 system.[49] Therefore, this implies a more complex picture compared to copper- or silver- single modified TiO_2. The presence of graphene in the specimens certainly affected this behaviour. In Table 3 are listed the time needed to halve the initial extent of the integrated area due to Cu^{2+} *d–d* electronic transitions (decreases), and the IFCT/Cu_2O integrated area (increases) – this is graphically shown in Figure S9. Including 0.5 wt% graphene (**Cu-G0.5/450**) for instance, favoured the kinetic of Cu^{2+} reduction, this being increased of a factor three (*i.e.*, 2.01 *versus* 5.93 min for **Cu-G0.5/450** and a copper-TiO_2 – *cf* Figure S10 for a visual comparison). The time needed to halve the IFCT-growth and the Cu_2O-generation/growth bands was 5.34 min *versus* 7.19 min on a 1 mol% Cu-TiO_2.

Presence of graphene in the system is a crucial factor for explaining that faster (photocatalytic / IFCT assisted) change in colour. As shown in Figure X4, white-light exposure induces IFCT between the valence band of TiO_2 and CuO clustered at its surface (orange full arrow). At the same time, an exciton is also generated: an electron is promoted from the valence band to the conduction band of TiO_2 (yellow dashed arrow). A conduction band transferring from TiO_2 to CuO is then favoured (yellow dotted arrow), thus further reducing Cu^{2+} to Cu^{+}. Moreover, the working function of graphene has a more positive value than the conduction band minimum of TiO_2 (*i.e.*, –4.5 eV *versus* –3.9 eV, respectively).[50,51] It is thus energetically feasible for the photogenerated electron to transfer itself from the conduction band of TiO_2 to graphene (left side of Figure X4). Graphene can act as a sink for the photogenerated electron, retarding the exciton recombination and favouring the electron transport in that system,[22] therefore the photocatalytic / IFCT driven change in colour.

Table 3 – Comparison of the time needed to halve ($t_{1/2}$) the initial integrated area of the absorption bands due to Cu^{2+} *d–d* transitions and IFCT/Cu_2O.

Sample	$t_{1/2}$ (min)	
	Cu^{2+} *d–d* transitions	IFCT/Cu_2O
Cu-TiO_2	5.93	7.19
Cu-G0.5/450	2.01	5.34
Cu-G1.0/450	2.30	6.94

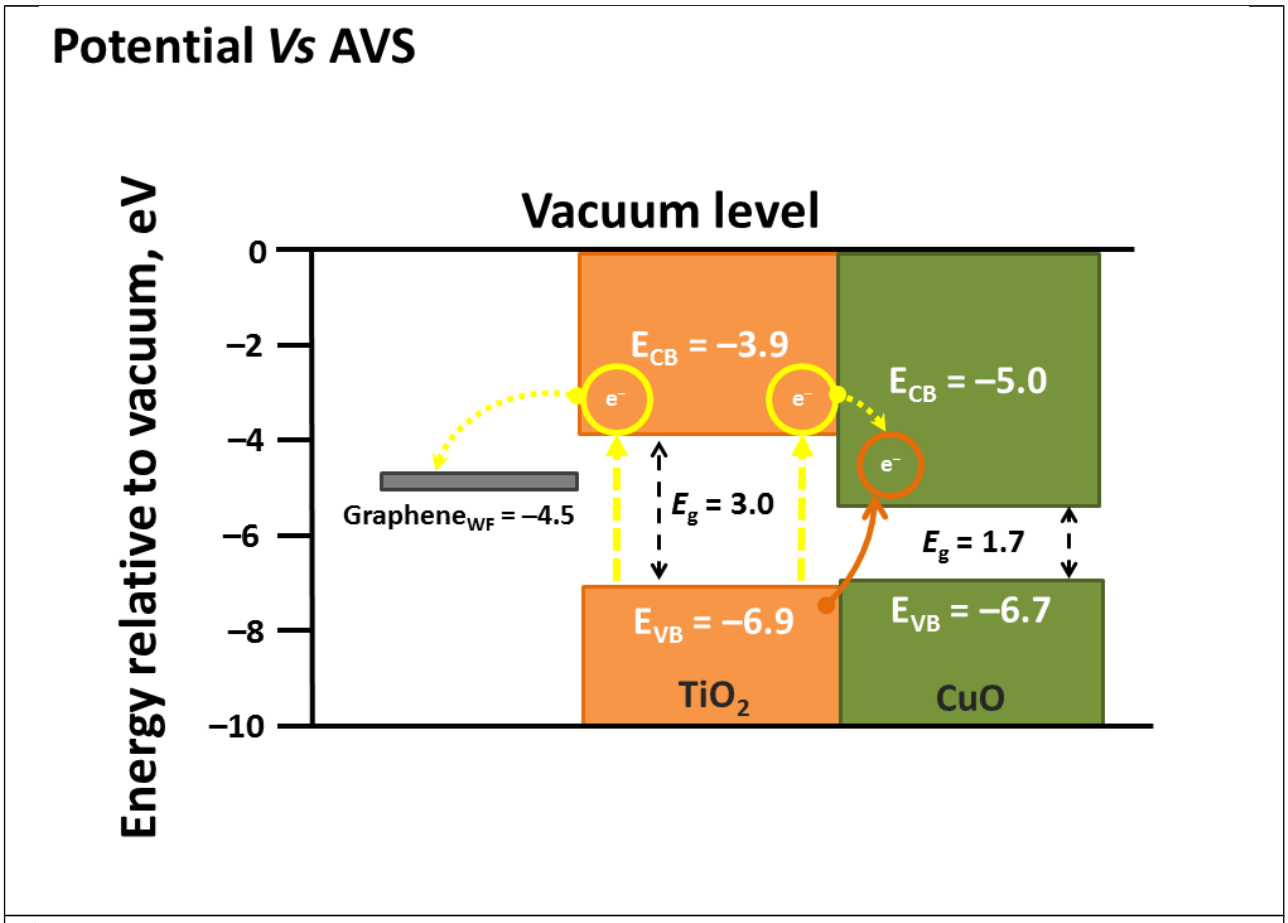

Figure X4 – Proposed mechanism for the visible-light induced photochromism in Cu-graphene-TiO_2. In the band diagram, the full orange arrow shows the electron transferring due to IFCT; dashed yellow arrows represent the electron transferring due to photocatalysis. Energy levels of TiO_2 and CuO are from Xu and Schoonen,[50] the value for the working function (WF) of graphene is from Liang and Ang.[51] The band-gap of TiO_2 has been calculated with the differential reflectance method (specimen **Cu-G1.0/450**).[27]

3.2.1 Reversible photochromic switches

Photochromic switching results are displayed in Figure S11 and Figure X5. Given the results described in *Section 3.2*, only specimens thermally treated at 450 °C / 2h (**Cu-G0.5/450** and **Cu-G1.0/450**) were analysed. In Figure S11 are reported the photochromic switching of the specimens that underwent 30 s vis-light irradiation time and 15 min at 100 °C to anneal and reverse the colour. Both the specimens displayed a clear and repeatable gap in the photochromic switching, showing a high degree of stability and repeatability up to a total of 14 cycles. Looking at Figure S11c, it is noticeable that specimen with 1.0 wt% graphene showed a recovery after the first cycle closer to the starting point, this suggesting that the high thermal conductivity of graphene aided the specimens to reverse their colour to the initial state. However, even though the switching cycles showed to be stable just after the second cycle, there was not a complete recovery to the initial value. Both the specimens exhibited a partial recovery of the initial virgin state after being annealed in the dark at 100 °C for 15 min. This meaning that annealing the specimens at 100 °C for 15 minutes was not enough to get a complete recovery of the initial virgin state.

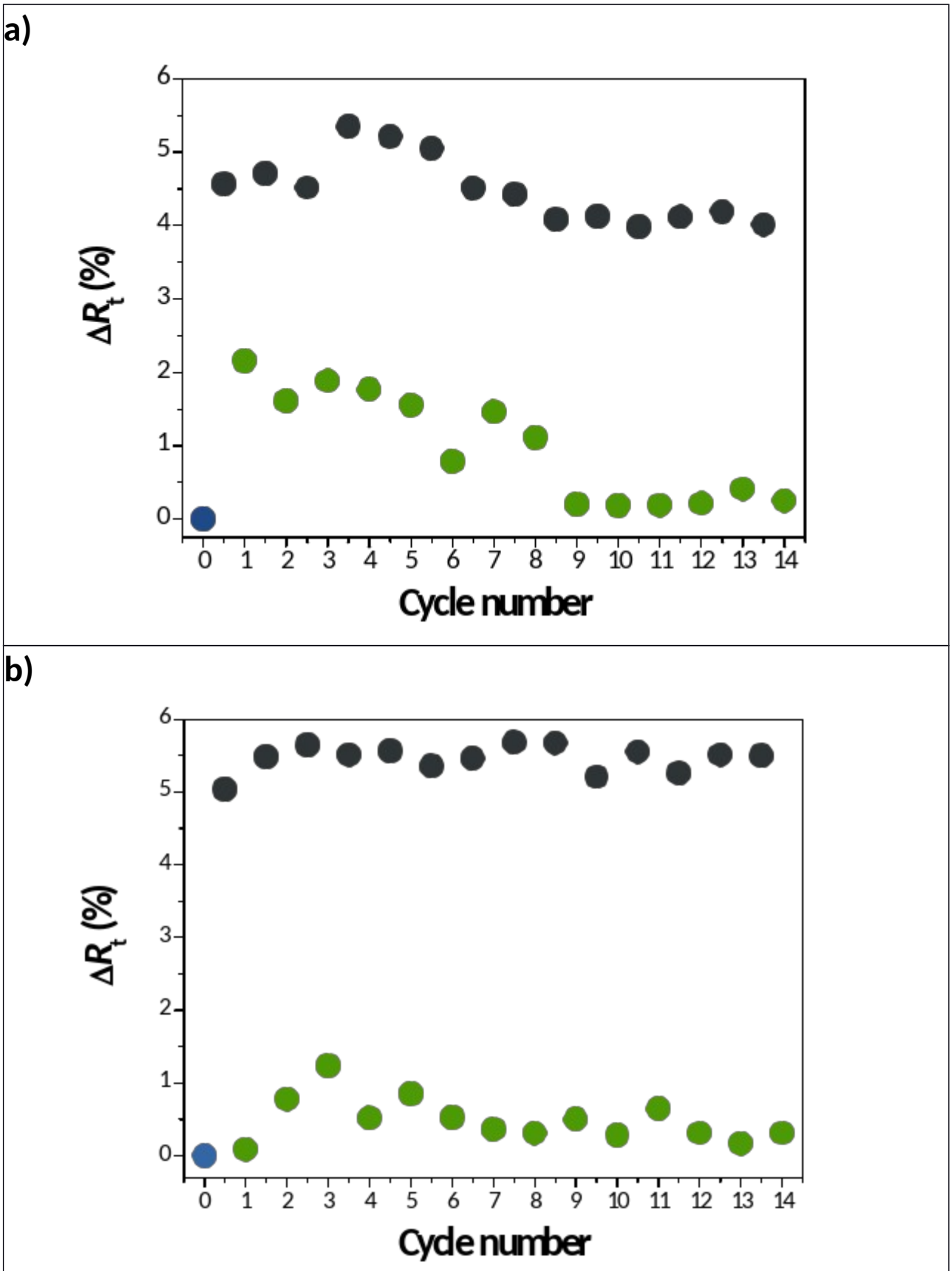

Figure X5 – a) **Cu-G0.5/450** photochromic recovery switches with repeated 15 s visible light irradiation (dark grey circles)/dark @ 100 °C for 30 min (green circles) cycles; the blue sphere represents the unexposed specimen. b) **Cu-G1.0/450** photochromic recovery switches with repeated 15 s visible light irradiation (dark grey circles)/dark @ 100 °C for 30 min (green circles) cycles; the blue circle represents the unexposed specimen.

In Figure X5 are reported the photochromic switching cycles for the specimens **Cu-G0.5/450** and **Cu-G1.0/450** subjected to 15 s white-light exposure, and annealed at 100 °C for 30 min. Here, it is clearly noticeable that the time granted for the annealing (30 min) was enough to fully reverse the photocatalytic / IFCT induced change in colour. Furthermore, the specimen with 1.0 wt% graphene (**Cu-G1.0/450**) showed to fully recover to the initial virgin state, thus confirming the positive two-fold influence of graphene on such a system – (i) electric transport for a fast photocatalytic / IFCT induced change in colour, and (ii) thermal conductivity to fully reverse that change in colour.

Conclusions

In this research work, we have produced a visible-light induced, photocatalytic / IFCT driven, all-inorganic switchable photochromic material. We have exploited the ability of TiO_2 (a mixture of anatase-rutile polymorphs) to generate an exciton upon light excitation. We have decorated the surface of TiO_2 nanoparticles with copper, the chromophore, and employed graphene's extraordinarily high electron mobility, as well as thermal conductivity, to create a "highway" for electron transport – and retarding the exciton recombination. We have shown that visible-light initiated cooperative photocatalytic / IFCT phenomena, which in turn induced a (reversible) change in colour to the material. Presence of graphene in the system boosted the photocatalytic / IFCT colour switching activation along with stability and reversibility of the colour switching. The photochromic switching of our material was shown to be stable and fully reversible – in case of **Cu-G1.0/450**. Our work could promote wide-scale applications of copper/graphene modified TiO_2 and initiate a further lap in visible-light activated reversible colour switching systems based on cooperative photocatalytic / IFCT mechanisms.

Acknowledgements

This work was partly developed within the scope of the bilateral project between Portugal and Slovakia, FCT/484/15/01/2019/S and in the frame of the project CICECO–Aveiro Institute of Materials, UIDB/50011/2020 & UIDP/50011/2020, financed by national funds through the FCT/MEC and when appropriate co-financed by FEDER under the PT2020 Partnership Agreement. David Maria Tobaldi is grateful to Portuguese national funds (OE), through FCT, I.P., in the scope of the framework contract foreseen in the numbers 4, 5 and 6 of the article 23, of the Decree-Law 57/2016, of August 29, changed by Law 57/2017, of July 19. We are obliged to Miss Dafne Maria Glaglanon for proof-editing the English of the manuscript.

References

(1) Zhang, J.; Zou, Q.; Tian, H. Photochromic Materials: More Than Meets The Eye. *Adv. Mater.* **2013**, *25* (3), 378–399. https://doi.org/10.1002/adma.201201521.

(2) Vik, M.; Periyasamy, A. P.; Viková, M. *Chromic Materials: Fundamentals, Measurements, and Applications*; 2019.

(3) Bamfield, P. *Chromic Phenomena*; 2010. https://doi.org/10.1039/9781849731034.

(4) He, T.; Yao, J. Photochromism in Composite and Hybrid Materials Based on Transition-Metal Oxides and Polyoxometalates. *Prog. Mater. Sci.* **2006**, *51* (6), 810–879. https://doi.org/10.1016/j.pmatsci.2005.12.001.

(5) Kamada, K.; Tanaka, Y.; Tokunaga, M.; Ueda, T.; Hyodo, T.; Shimizu, Y. Multicolour Photochromism of Colloidal Solutions of Niobate Nanosheets Intercalated with Several Kinds of Metal Ions. *Chem. Commun.* **2016**. https://doi.org/10.1039/C5CC09270A.

(6) Tobaldi, D. M.; Hortigüela Gallo, M. J.; Otero-Irurueta, G.; Singh, M. K.; Pullar, R. C.; Seabra, M. P.; Labrincha, J. A. Purely Visible-Light-Induced Photochromism in Ag–TiO2 Nanoheterostructures. *Langmuir* **2017**, *33* (20), 4890–4902. https://doi.org/10.1021/acs.langmuir.6b04474.

(7) Bouas-Laurent, H.; Dürr, H. Organic Photochromism (IUPAC Technical Report). *Pure Appl. Chem.* **2001**, *73* (4), 639–665. https://doi.org/10.1351/pac200173040639.

(8) Fredrich, S.; Göstl, R.; Herder, M.; Grubert, L.; Hecht, S. Switching Diarylethenes Reliably in Both Directions with Visible Light. *Angew. Chem. Int. Ed Engl.* **2016**, *55* (3), 1208–1212. https://doi.org/10.1002/anie.201509875.

(9) Mukhopadhyay, A.; Moorthy, J. N. Phenomenon to Functions: Photochromism of Diarylpyrans, Spectrokinetic Properties and Functional Materials. *J. Photochem. Photobiol. C Photochem. Rev.* **2016**, *29* (Supplement C), 73–106. https://doi.org/10.1016/j.jphotochemrev.2016.11.002.

(10) Nigra, A. E.; Ruiz-Hernandez, A.; Redon, J.; Navas-Acien, A.; Tellez-Plaza, M. Environmental Metals and Cardiovascular Disease in Adults: A Systematic Review Beyond Lead and Cadmium. *Curr. Environ. Health Rep.* **2016**, *3* (4), 416–433. https://doi.org/10.1007/s40572-016-0117-9.

(11) Fujishima, A.; Honda, K. Electrochemical Photolysis of Water at a Semiconductor Electrode. *Nature* **1972**, *238* (5358), 37–38. https://doi.org/10.1038/238037a0.

(12) Wang, W.; Xie, N.; He, L.; Yin, Y. Photocatalytic Colour Switching of Redox Dyes for Ink-Free Light-Printable Rewritable Paper. *Nat. Commun.* **2014**, *5* (1), 5459. https://doi.org/10.1038/ncomms6459.

(13) Wang, W.; Liu, L.; Feng, J.; Yin, Y. Photocatalytic Reversible Color Switching Based on Titania Nanoparticles. *Small Methods* **2018**, *2* (2), 1700273. https://doi.org/10.1002/smtd.201700273.

(14) Scanlon, D. O.; Dunnill, C. W.; Buckeridge, J.; Shevlin, S. A.; Logsdail, A. J.; Woodley, S. M.; Catlow, C. R. A.; Powell, M. J.; Palgrave, R. G.; Parkin, I. P.; et al. Band Alignment of Rutile and Anatase TiO2. *Nat. Mater.* **2013**, *12* (9), 798–801. https://doi.org/10.1038/nmat3697.

(15) Maheu, C.; Cardenas, L.; Puzenat, E.; Afanasiev, P.; Geantet, C. UPS and UV Spectroscopies Combined to Position the Energy Levels of TiO2 Anatase and Rutile Nanopowders. *Phys. Chem. Chem. Phys.* **2018**, *20* (40), 25629–25637. https://doi.org/10.1039/C8CP04614J.

(16) Mo, S.-D.; Ching, W. Y. Electronic and Optical Properties of Three Phases of Titanium Dioxide: Rutile, Anatase, and Brookite. *Phys. Rev. B* **1995**, *51* (19), 13023–13032. https://doi.org/10.1103/PhysRevB.51.13023.

(17) Gawande, M. B.; Goswami, A.; Felpin, F.-X.; Asefa, T.; Huang, X.; Silva, R.; Zou, X.; Zboril, R.; Varma, R. S. Cu and Cu-Based Nanoparticles: Synthesis and Applications in Catalysis. *Chem. Rev.* **2016**, *116* (6), 3722–3811. https://doi.org/10.1021/acs.chemrev.5b00482.

(18) Novoselov, K. S.; Geim, A. K.; Morozov, I. V.; Jiang, D.; Zhang, Y, Y.; Dubonos, S. V.; Grigorieva, I. V.; Firsov, A. A. Electric Field Effect in Atomically Thin Carbon Films. *Science* **2004**, *306* (5696), 666–669. https://doi.org/10.1126/science.1102896.

(19) Geim, A. K.; Novoselov, K. S. The Rise of Graphene. *Nat. Mater.* **2007**, *6* (3), 183–191. https://doi.org/10.1038/nmat1849.

(20) Novoselov, K. S.; Blake, P.; Katsnelson, M. I. Graphene: Electronic Properties. In *Encyclopedia of Materials: Science and Technology*; Buschow, K. H. J., Cahn, R. W., Flemings, M. C., Ilschner, B., Kramer,

E. J., Mahajan, S., Veyssière, P., Eds.; Elsevier: Oxford, 2008; pp 1–6. https://doi.org/10.1016/B978-008043152-9.02191-6.
(21) Novoselov, K. S.; Geim, A. K.; Morozov, S. V.; Jiang, D.; Katsnelson, M. I.; Grigorieva, I. V.; Dubonos, S. V.; Firsov, A. A. Two-Dimensional Gas of Massless Dirac Fermions in Graphene. *Nature* **2005**, *438* (7065), 197–200. https://doi.org/10.1038/nature04233.
(22) Morozov, S. V.; Novoselov, K. S.; Katsnelson, M. I.; Schedin, F.; Elias, D. C.; Jaszczak, J. A.; Geim, A. K. Giant Intrinsic Carrier Mobilities in Graphene and Its Bilayer. *Phys. Rev. Lett.* **2008**, *100* (1), 016602. https://doi.org/10.1103/PhysRevLett.100.016602.
(23) Balandin, A. A. Thermal Properties of Graphene and Nanostructured Carbon Materials. *Nat. Mater.* **2011**, *10* (8), 569–581. https://doi.org/10.1038/nmat3064.
(24) Kamat, P. V. Graphene-Based Nanoarchitectures. Anchoring Semiconductor and Metal Nanoparticles on a Two-Dimensional Carbon Support. *J. Phys. Chem. Lett.* **2010**, *1* (2), 520–527. https://doi.org/10.1021/jz900265j.
(25) Tobaldi, D. M.; Leonardi, S. G.; Movlaee, K.; Lajaunie, L.; Seabra, M. P.; Arenal, R.; Neri, G.; Labrincha, J. A. Hybrid Noble-Metals/Metal-Oxide Bifunctional Nano-Heterostructure Displaying Outperforming Gas-Sensing and Photochromic Performances. *ACS Omega* **2018**, *3* (8), 9846–9859. https://doi.org/10.1021/acsomega.8b01508.
(26) Tobaldi, D. M.; Rozman, N.; Leoni, M.; Seabra, M. P.; Škapin, A. S.; Pullar, R. C.; Labrincha, J. A. Cu–TiO_2 Hybrid Nanoparticles Exhibiting Tunable Photochromic Behavior. *J. Phys. Chem. C* **2015**, *119* (41), 23658–23668. https://doi.org/10.1021/acs.jpcc.5b07160.
(27) Tobaldi, D. M.; Lajaunie, L.; Rozman, N.; Caetano, A. P. F.; Seabra, M. P.; Sever Škapin, A.; Arenal, R.; Labrincha, J. A. Impact of the Absolute Rutile Fraction on TiO2 Visible-Light Absorption and Visible-Light-Promoted Photocatalytic Activity. *J. Photochem. Photobiol. Chem.* **2019**, *382*, 111940. https://doi.org/10.1016/j.jphotochem.2019.111940.
(28) Larson, A. C.; Von Dreele, R. B. *General Structure Analysis System (GSAS)*; Los Alamos National Laboratory Report LAUR, 2004.
(29) Toby, B. H. EXPGUI, a Graphical User Interface for GSAS. *J. Appl. Crystallogr.* **2001**, *34* (2), 210–213. https://doi.org/10.1107/S0021889801002242.
(30) Scardi, P.; Leoni, M. Whole Powder Pattern Modelling. *Acta Crystallogr. A* **2002**, *58* (2), 190–200. https://doi.org/10.1107/S0108767301021298.
(31) Leoni, M.; Confente, T.; Scardi, P. PM2K: A Flexible Program Implementing Whole Powder Pattern Modelling. *Z. Für Krist. Suppl.* **2006**, *23* (suppl_23_2006), 249–254. https://doi.org/10.1524/zksu.2006.suppl_23.249.
(32) Scardi, P.; Ortolani, M.; Leoni, M. WPPM: Microstructural Analysis beyond the Rietveld Method. *Mater. Sci. Forum* **2010**, *651*, 155–171. https://doi.org/10.4028/www.scientific.net/MSF.651.155.
(33) Tobaldi, D. M.; Lajaunie, L.; López Haro, M.; Ferreira, R. A. S.; Leoni, M.; Seabra, M. P.; Calvino, J. J.; Carlos, L. D.; Labrincha, J. A. Synergy of Neodymium and Copper for Fast and Reversible Visible-Light Promoted Photochromism, and Photocatalysis, in Cu/Nd-TiO2 Nanoparticles. *ACS Appl. Energy Mater.* **2019**, *2* (5), 3237–3252. https://doi.org/10.1021/acsaem.9b00084.
(34) Marfunin, A. S. *Physics of Minerals and Inorganic Materials: An Introduction*; Springer-Verlag, 1979.
(35) Sun, H.; Liu, J.; Wang, X.; Zhang, Q.; Hao, X.; An, S. (K,Na)NbO3 Ferroelectrics: A New Class of Solid-State Photochromic Materials with Reversible Luminescence Switching Behavior. *J. Mater. Chem. C* **2017**. https://doi.org/10.1039/C7TC03076B.
(36) Giampiccolo, A.; Tobaldi, D. M.; Leonardi, S. G.; Murdoch, B. J.; Seabra, M. P.; Ansell, M. P.; Neri, G.; Ball, R. J. Sol Gel Graphene/TiO2 Nanoparticles for the Photocatalytic-Assisted Sensing and Abatement of NO2. *Appl. Catal. B Environ.* **2019**, *243*, 183–194. https://doi.org/10.1016/j.apcatb.2018.10.032.
(37) Shannon, R. D.; Pask, J. A. Kinetics of the Anatase-Rutile Transformation. *J. Am. Ceram. Soc.* **1965**, *48* (8), 391–398. https://doi.org/10.1111/j.1151-2916.1965.tb14774.x.
(38) Bhattacharjee, S. DLS and Zeta Potential – What They Are and What They Are Not? *J. Controlled Release* **2016**, *235*, 337–351. https://doi.org/10.1016/j.jconrel.2016.06.017.

(39) Tobaldi, D. M.; Pullar, R. C.; Binions, R.; Jorge, A. B.; McMillan, P. F.; Saeli, M.; Seabra, M. P.; Labrincha, J. A. Influence of Sol Counter-Ions on the Visible Light Induced Photocatalytic Behaviour of TiO2 Nanoparticles. *Catal. Sci. Technol.* **2014**, *4* (7), 2134–2146. https://doi.org/10.1039/C4CY00423J.
(40) Li Bassi, A.; Cattaneo, D.; Russo, V.; Bottani, C. E.; Barborini, E.; Mazza, T.; Piseri, P.; Milani, P.; Ernst, F. O.; Wegner, K.; et al. Raman Spectroscopy Characterization of Titania Nanoparticles Produced by Flame Pyrolysis: The Influence of Size and Stoichiometry. *J. Appl. Phys.* **2005**, *98* (7), 074305. https://doi.org/doi:10.1063/1.2061894.
(41) Coates, J. Interpretation of Infrared Spectra, A Practical Approach. In *Encyclopedia of Analytical Chemistry*; John Wiley & Sons, Ltd, 2006. https://doi.org/10.1002/9780470027318.a5606.
(42) Ferrari, A. C.; Meyer, J. C.; Scardaci, V.; Casiraghi, C.; Lazzeri, M.; Mauri, F.; Piscanec, S.; Jiang, D.; Novoselov, K. S.; Roth, S.; et al. Raman Spectrum of Graphene and Graphene Layers. *Phys. Rev. Lett.* **2006**, *97* (18), 187401. https://doi.org/10.1103/PhysRevLett.97.187401.
(43) Bose, S. M.; Gayen, S.; Behera, S. N. Theory of the Tangential G -Band Feature in the Raman Spectra of Metallic Carbon Nanotubes. *Phys. Rev. B* **2005**, *72* (15), 153402. https://doi.org/10.1103/PhysRevB.72.153402.
(44) Burns, R. G. *Mineralogical Applications of Crystal Field Theory*; Cambridge University Press, 1993.
(45) Irie, H.; Kamiya, K.; Shibanuma, T.; Miura, S.; Tryk, D. A.; Yokoyama, T.; Hashimoto, K. Visible Light-Sensitive Cu(II)-Grafted TiO_2 Photocatalysts: Activities and X-Ray Absorption Fine Structure Analyses. *J. Phys. Chem. C* **2009**, *113* (24), 10761–10766. https://doi.org/10.1021/jp903063z.
(46) Huang, Q.; Tian, S.; Zeng, D.; Wang, X.; Song, W.; Li, Y.; Xiao, W.; Xie, C. Enhanced Photocatalytic Activity of Chemically Bonded TiO2/Graphene Composites Based on the Effective Interfacial Charge Transfer through the C–Ti Bond. *ACS Catal.* **2013**, *3* (7), 1477–1485. https://doi.org/10.1021/cs400080w.
(47) *Spectroscopic Methods in Mineralogy and Geology*; Hawthorne, F. C., Mineralogical Society of America, Eds.; Mineralogical Society of America: Washington, D.C., 1988.
(48) Banerjee, S.; Chakravorty, D. Optical Absorption by Nanoparticles of Cu_2O. *Europhys. Lett. EPL* **2000**, *52* (4), 468–473. https://doi.org/10.1209/epl/i2000-00461-5.
(49) Serra, A.; Manno, D.; Buccolieri, A.; Carbone, G. G.; Calcagnile, L. Photochromic Properties in Silver-Doped Titania Nanoparticles. *Mater. Res. Express* **2018**, *6* (3), 036206. https://doi.org/10.1088/2053-1591/aaf816.
(50) Xu, Y.; Schoonen, M. A. A. The Absolute Energy Positions of Conduction and Valence Bands of Selected Semiconducting Minerals. *Am. Mineral.* **2000**, *85* (3–4), 543–556.
(51) Liang, S.-J.; Ang, L. K. Electron Thermionic Emission from Graphene and a Thermionic Energy Converter. *Phys. Rev. Appl.* **2015**, *3* (1), 014002. https://doi.org/10.1103/PhysRevApplied.3.014002.